

RSC Advances



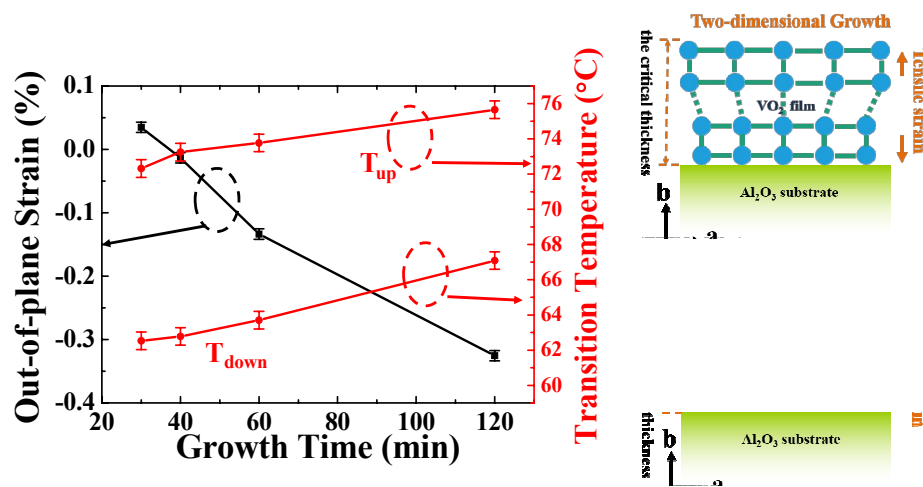
This is an *Accepted Manuscript*, which has been through the Royal Society of Chemistry peer review process and has been accepted for publication.

Accepted Manuscripts are published online shortly after acceptance, before technical editing, formatting and proof reading. Using this free service, authors can make their results available to the community, in citable form, before we publish the edited article. This *Accepted Manuscript* will be replaced by the edited, formatted and paginated article as soon as this is available.

You can find more information about *Accepted Manuscripts* in the [Information for Authors](#).

Please note that technical editing may introduce minor changes to the text and/or graphics, which may alter content. The journal's standard [Terms & Conditions](#) and the [Ethical guidelines](#) still apply. In no event shall the Royal Society of Chemistry be held responsible for any errors or omissions in this *Accepted Manuscript* or any consequences arising from the use of any information it contains.

Graphical abstracts



The anomalous compressive strain is observed in thicker $\text{VO}_2/\text{Al}_2\text{O}_3$ epitaxial films, which is ascribed to the surface growth mode. However, the formation mechanism of the strain in the thinner $\text{VO}_2/\text{Al}_2\text{O}_3$ epitaxial films can be explained by conventional epitaxial lattice-mismatch. Strain engineering may be served as an effective avenue for manipulating MIT behaviors of the VO_2 epitaxial films.

Surface-growth-mode-induced Strain Effects on the Metal-Insulator Transition in Epitaxial Vanadium Dioxide Thin Films

Mengmeng Yang¹, Yuanjun Yang^{1,2,*}, Bin Hong^{1,2}, Liangxin Wang¹, Zhenlin Luo¹, Xiaoguang Li³, Chaoyang Kang⁴, Ming Li⁴, Haitao Zong⁴, Chen Gao^{1,2,*}

¹*National Synchrotron Radiation Laboratory & Collaborative Innovation Center of Chemistry for Energy Materials, University of Science and Technology of China, Hefei, Anhui 230026, China*

²*CAS Key Laboratory of Materials for Energy Conversion, Department of Materials Science and Engineering, University of Science and Technology of China, Hefei, Anhui 230026, China*

³*Hefei National Laboratory for Physical Sciences at the Microscale and Department of Physics, University of Science and Technology of China, Hefei, Anhui 230026, China*

⁴*School of Physics and Chemistry, Henan Polytechnic University, Jiaozuo, Henan 454000, China*

*Corresponding Author. Fax: (+86)551-65141078. Tel: (+86)551-63602031.

Email address: yangyuanjun@ustc.edu.cn or cgao@ustc.edu.cn.

ABSTRACT

A series of high-quality vanadium dioxide (VO_2) epitaxial thin films on (0001)-oriented sapphire substrates with various thicknesses were fabricated using radio frequency (RF) magnetron sputtering techniques. Structural analysis revealed that an out-of-plane tensile strain ($\sim+0.035\%$) in the thinner VO_2 epitaxial films was induced by epitaxial lattice mismatch between the monoclinic VO_2 films and Al_2O_3 substrates. However, an anomalous compressive strain ($\sim-0.32\%$) was accumulated along the out-of-plane direction in the thicker VO_2 films. This result contradicts with the conventional epitaxial lattice-mismatch mechanism for strain formed in epitaxial films. We attribute this anomalous strain to the surface growth mode (island growth) in the thicker VO_2 films, especially those sputtered from the metal target at low pressure. Furthermore, the metal-insulator transition (MIT) temperature shifted to lower temperature with decreasing thickness, which is attributed to modulation of the orbital occupancy through the epitaxial strain and growth-mode-induced strain in the VO_2 epitaxial films. Moreover, the very large resistance change (on the order of magnitude $\sim 10^3$) in the $\text{VO}_2/\text{Al}_2\text{O}_3$ epitaxial heterostructures is promising for electrical switch applications.

Keywords: VO_2 ; epitaxial thin film; strain effects; metal-insulator transition; surface growth mode

1 Introduction

Since Morin discovered vanadium dioxide (VO_2) exhibiting a first-order phase transition from a monoclinic to a tetragonal crystalline structure at approximately 68 °C in 1959¹, researchers worldwide have been investigating the mechanism which is responsible for the phase transition. The phase transition well known as metal-insulator transition (MIT) can be triggered not only by temperature² but also by an electric field³, light^{4,5}, and strain^{6,7}. The phase transition is accompanied by abrupt several-orders-of-magnitude changes in the optical and electrical properties of VO_2 . These properties make VO_2 a promising candidate for various applications, such as smart windows⁸⁻¹⁰ and lithium-ion battery^{11,12}.

The thin film of a material is often grown on a certain substrate. Single-crystal TiO_2 and Al_2O_3 substrates are most commonly used for growing high-quality epitaxial VO_2 thin films.¹³⁻²² Therefore, strains due to lattice mismatches between the VO_2 thin films and TiO_2 and Al_2O_3 substrates must be considered, especially for practical applications based on VO_2 thin films. In addition, the strain provides another freedom to manipulate the metal-insulator transition.^{17,18} Recently, TiO_2 substrates were chosen for growing epitaxial VO_2 films, where the considerable epitaxial strain can be sustained across the entire thickness of the material due to the relative small lattice mismatch ($\sim -0.65\%$) between the VO_2 thin films and TiO_2 substrates. For example, Parkin *et al.*²⁰ changed the MIT temperature of $\text{VO}_2/\text{RuO}_2/\text{TiO}_2$ films from ~ 12 °C to ~ 72 °C by varying the thickness of the RuO_2 buffer layer (thus resulting in different epitaxial strains in the VO_2 thin films). L. L. Fan *et al.*²¹ studied the strain states in

VO₂/TiO₂ epitaxial films by changing the VO₂ film thickness and claimed that the electronic orbital occupancy was strongly affected by the interfacial strain. Although there have been many studies focused on the strain states in the typical VO₂/TiO₂ hetero-epitaxial system, there are few systematic studies of the strain states in VO₂/Al₂O₃ system. Recently, Tsung-Han Yang *et al.*¹⁶ deposited VO₂ thin films grown on c- and r-sapphire substrates using RF-magnetron sputtering and attributed the modulation of the MIT to the strain between the film and substrate. However, they didn't study the thickness-dependent strain effect on the MIT behaviors in the VO₂/Al₂O₃ epitaxial films. Because of the large lattice mismatch (~13%) and angle mismatch between the VO₂ (monoclinic) and Al₂O₃ (rhombohedral) substrate, the strain rapidly relaxes above the critical thickness (~2.1 nm) in the viewpoint of the hetero-epitaxial system.²³ Therefore, the strain states of epitaxial VO₂/Al₂O₃ thin films have not been considered in detail. The role of strain freedom in the MIT of this system is not yet fully understood.

On the other hand, the underlying physics of the MIT of VO₂ thin films is still debated among the prominent theories involving a thermal-driven structural phase transition²⁴, an electron-correlation-driven Mott²⁵ and coactions of these two mechanisms²⁶. Recently, S. Kittiwatanakul *et al.*²⁷ reported that a large epitaxial bi-axial strain induced a Mott-like phase transition without the concomitant Peierls transition in the hetero-epitaxial system of VO₂/TiO₂ thin films, which is similar to our findings (which are currently unpublished). This finding indicates that the strain may suppress the structural phase transition and even alter the electronic structure of

the VO₂, which makes us re-examine and further understand the mechanism of the MIT of strained VO₂ thin films.

Motivated by the above studies, in this work, we prepared a series of high-quality VO₂ epitaxial films of various thicknesses grown on (0001)-Al₂O₃ substrates (*c* oriented) using RF-magnetron sputtering technique. Another reason for the choice of Al₂O₃ substrate is of wide availability for fabricating high quality epitaxial VO₂ films on it. The strain evolutions were investigated in the different thickness VO₂ films. We reported anomalous strain states in this VO₂/Al₂O₃ system, which have not been observed previously and ascribed the reason to the specific surface growth mode.

2 Experimental Procedures

2.1 Film growth and thickness characterization

A series of VO₂ thin films of different thicknesses were deposited on commercial single (0001)-oriented Al₂O₃ substrates via RF-magnetron sputtering. The base pressure was pumped to 2×10^{-4} Pa. A vanadium metal target (99.99% purity) was sputtered at a 60 W RF power and sputtering pressure of 0.43 Pa with an Ar:O₂ (99.99%) flow ratio of 60:0.5.¹⁹ The growth temperature was set to 350 °C, and the growth times were 15, 20, 30 and 60 min for the VO₂ thin films with various thicknesses, respectively.

The thickness measurement was conducted via small angle X-ray reflectivity (XRR) measurement, which is an effective non-destructive tool to measure the

thickness. With XRR, we have determined the thickness of all samples.

2.2 Structure characterization

The structure and quality of the VO₂ films were characterized by high-resolution XRD with Cu K α ₁ ($\lambda=1.5406$ Å) radiation (Rigaku SmartLab Film Version), and the partial structure information was obtained from the 14B beamline of the Shanghai Synchrotron Radiation Facilities with the reciprocal space mapping (RSM) technology. The structural phase transition across the MIT of the VO₂ thin films was investigated by *in situ* temperature-dependent XRD. XRD scans were performed when the *in situ* temperature was stable.

2.3 Surface morphology characterization

The surface morphology of the VO₂ thin films were examined by the Atomic Force Microscopy (AFM, Bruker Dimension Icon) in the ScanAsyst mode. Then the surface roughness values (root mean square) were obtained by averaging the total surface area in the AFM images.

2.4 Electrical transport measurements

With the help of the multifunction of Physical Properties Measurement System (PPMS, Quantum Design, Inc.), the hysteresis loops of the resistivity as a function of temperature were measured by four-probe method in the temperature range of 25~120 °C with the accuracy of 0.05 °C.

3 Results and Discussion

3.1 Epitaxiality characterization

To evaluate the quality of the VO₂ thin films, XRD patterns were acquired for a typical VO₂ thin film with thickness of ~60 nm and are presented in Fig. 1. As can be observed from Fig. 1(a), only (020) peak of the VO₂ film and three peaks of the Al₂O₃ substrate appeared, thereby indicating the high orientation and good purity of the VO₂ thin films. The inset of Fig. 1(a) is a typical X-ray reflectivity (XRR) curve showing the distinct interference fringes. The corresponding thickness can be calculated to be ~60 nm via Bragg formula.²¹ According to the rocking curve of the VO₂ (020) peak (see Fig. 1(b)), the full width at half maximum (FWHM) is only about 0.54°, which indicates the good quality of the VO₂ thin films.^{19,28} From the fine scanning curve shown in Fig. 1(c), it can be found that the VO₂ (020) peak and sapphire (0006) peaks locate at 39.955° and 41.685°, respectively, which is consistent with the results reported in ref. 29. The reciprocal space map (RSM) of the VO₂ (220) peak and Al₂O₃ (116) obtained after performing φ scans¹⁹ is presented in Fig. 1(d); it demonstrates the perfect epitaxial relationship between the VO₂ film and Al₂O₃ substrate. Consequently, the epitaxial relationship is derived to be $[101]_{\text{VO}_2} // [1\bar{1}\bar{2}0]_{\text{Al}_2\text{O}_3}$ along the in-plane direction and $[010]_{\text{VO}_2} // [0001]_{\text{Al}_2\text{O}_3}$ along the out-of-plane direction.^{28,29} Interestingly, the VO₂ (220) peak splits into three parts representing three different oriented domains, and we will discuss this result in another paper. We deposited four VO₂ films of different thicknesses with different growth times of 15, 20, 30 and 60 min, respectively. The thicknesses were determined to be ~30, ~40, ~60, and ~120 nm by non-destructive small angle X-ray reflectivity measurement (typically shown in the inset of Fig. 1(a)).

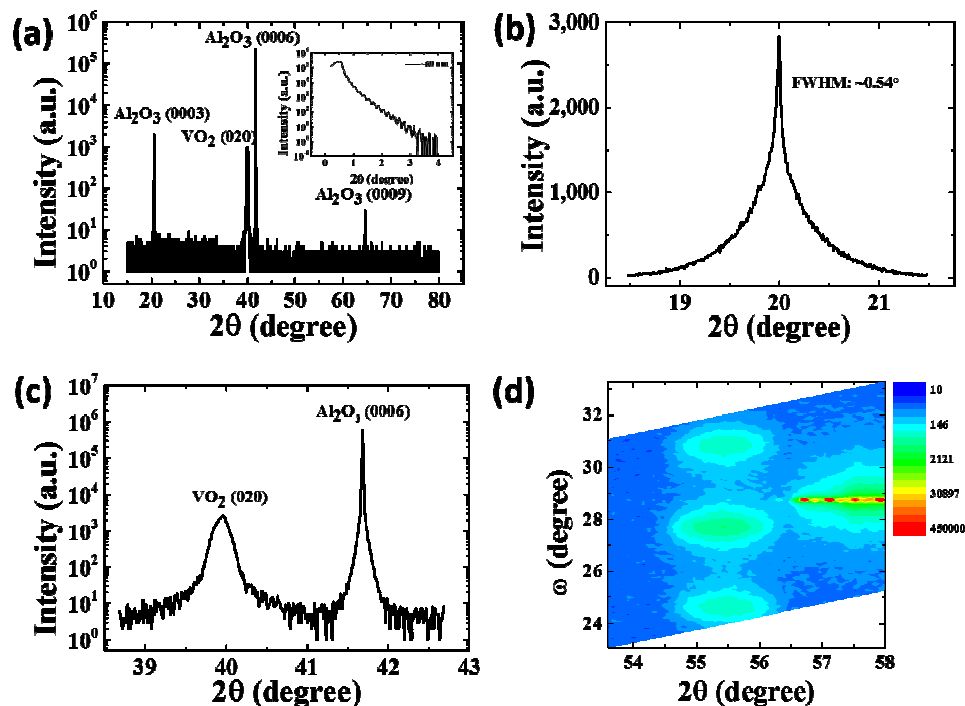


Fig. 1 (color online) (a) Typical θ - 2θ scan of the VO₂ film grown on c-Al₂O₃ substrate by RF magnetron sputtering, inset: the typical XRR curve of a 60 nm-thick VO₂ thin film. (b) Rocking curve of the VO₂ (020) peak. (c) Fine scan curve of the VO₂ (020) peak from 38.6° to 42.6°. (d) RSM maps of VO₂ (220) and Al₂O₃ (116).

3.2 Thickness-dependent MIT of the VO₂/Al₂O₃ epitaxial films

In order to analyze the MIT characteristics of the VO₂ thin films, the resistance-temperature (R-T) curves of the four samples were measured by PPMS. As shown in Fig. 2, during the temperature cycling from 25 to 120 °C and reversing back, the normalized resistances of 40, 60 and 120 nm samples increased by approximately three orders of magnitudes, showing an obvious and sharp transitions with the typical hysteresis appearing between the heating and cooling processes. The thinnest VO₂

film (~30 nm) also shows an obvious MIT; however, the change of resistance across the transition was most likely suppressed by strain in the film.²¹

The differentiations of the R-T curves obtained using the formula $d \log(R) / dT$ are presented in the insets of Fig. 2. As deduced from the minimum of each differentiation curve, the transition temperatures of the four samples were 60, 63, 64 and 67 °C during the cooling process and 71, 74, 72 and 75 °C during the heating process. It can be inferred from the multiple measurements and averaging the transition temperatures that the MIT temperatures has an increasing tendency with increasing thickness of the VO₂ film in a large content, which is shown in the red curves in Fig. 3(b).

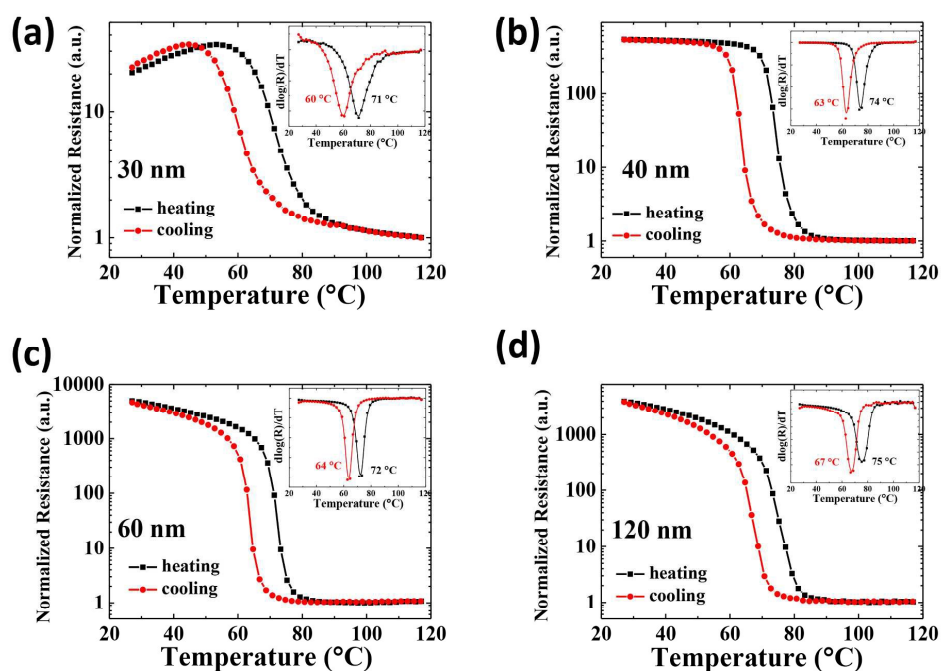


Fig. 2 (color online) R-T curves of the typical batch of the (a) 30-nm, (b) 40-nm, (c) 60-nm and (d) 120-nm samples measured by PPMS by single cycling temperature. Insets: differential curves of

each R-T curve for all four samples.

3.3 Origin of the thickness-dependent transition temperature

According to previous studies^{20,21,30}, modulation of the transition temperature across the MIT may be induced by interfacial strains between the VO₂ film and the substrate. Therefore, we attributed the change of transition temperature to the interfacial strain. We performed XRD θ - 2θ scans for the four VO₂ thin films with different thicknesses. The XRD patterns shown in Fig. 3(a) contain sharp peaks at 39.9° that are associated with the Al₂O₃ substrate (0006) peaks, which do not shift among the four samples. With increasing thickness, the VO₂ diffraction peak exhibits a clear shift to higher angles (2θ are 39.785°, 39.825°, 39.875° and 39.955° respectively, which is indicated by the guided line). According to Bragg's law, the lattice constant d_f were calculated to be 2.26389 Å, 2.2628 Å, 2.26008 Å and 2.25574 Å, respectively. Thus, the strain between the VO₂ thin film and the substrate is defined as:

$$strain = \frac{d_f - d_b}{d_b} \times 100\%, \quad (1)$$

where d_f and d_b ($d_b=2.2631$ Å) represent the lattice constants of the VO₂ thin film and the counterpart bulk one, respectively. Following this definition, the strain vs. thickness curve was obtained and is presented in Fig. 3(b). It can be found that the strain changes from tensile (conventionally positive) to compressive (and hence, negative) strain.

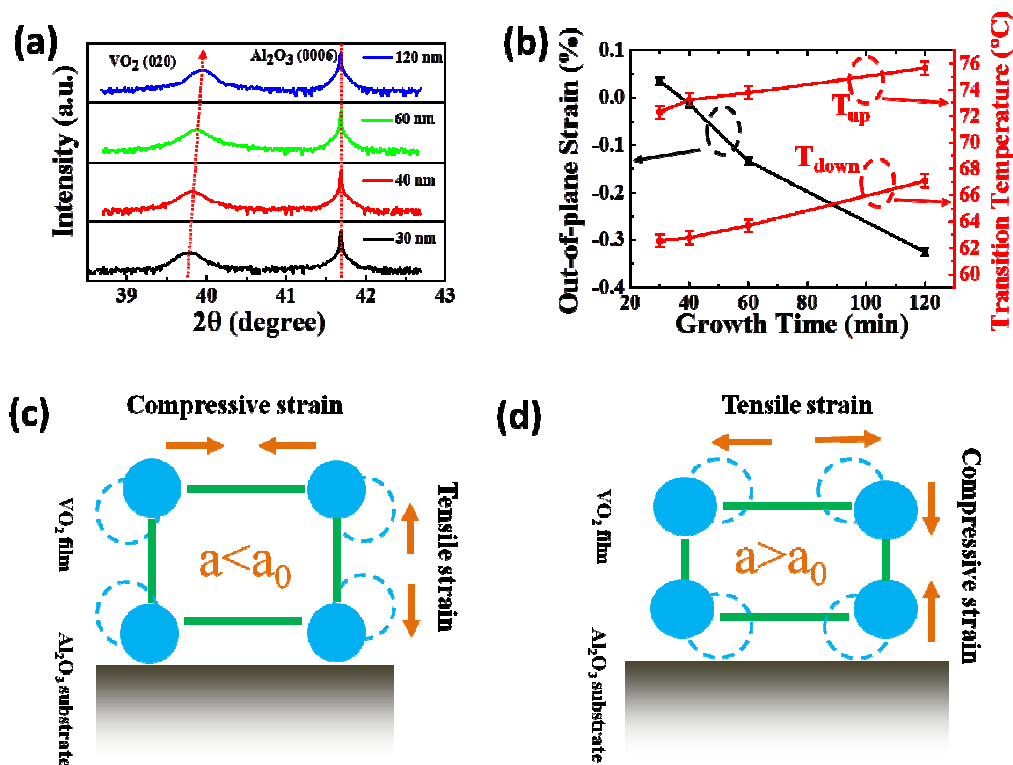


Fig. 3 (color online) (a) Fine θ - 2θ scans of the VO₂ (020) peaks of the four different thickness samples. The red guided line represents the peak shift. (b) The out-of-plane strain and transition temperature lines are plotted as a function of the sample thickness. The error bars base on the statistical average of the MIT temperature by multiple measurements. The schematic illustrations of the (c) tensile and (d) compressive strain along the out-of-plane direction in the thin and thick VO₂ thin films, respectively.

Comparing the three curves shown in Fig. 3(b), the transition temperature exhibits a tendency opposite to the strain both at heating and cooling process. It is believed that this behavior is modulated by the interfacial strain, which is consistent with the conclusions of ref. 20 and 21. The modulation mechanism is that the strain in the VO₂ film modifies the orbital occupancy near the Fermi energy level E_F . The

compressive strain along the out-of-plane direction causes the d_{\parallel} and π^* orbitals to shift upward and the d_{\parallel}^* orbital downward. Therefore, in the insulator state, the band gap increases by the out-of-plane compressive strain along the b_M direction in the (020)-VO₂ epitaxial film, the energy barrier increases and thus the MIT is triggered at higher temperature. Consequently, the electronic orbital occupancy changes due to the epitaxial strain, and the surface-growth-mode-induced strain modulates the phase transition behavior and triggers the onset of the MIT at higher temperature in the thicker and compressively strained VO₂/Al₂O₃ thin films.^{20,21}

It is noteworthy that the compressive strain state (Fig. 3(d)) along the out-of-plane direction is observed in the thicker films; however, a tensile strain exists in the thinnest film (Fig. 3 (c)). Moreover, the compressive strain becomes even stronger in the thicker films. From hetero-epitaxial system²³, only tensile but not compressive strain can be maintained in the VO₂/Al₂O₃ epitaxial films along the out-of-plane direction, which should be relaxed with increasing film thickness. As for the thinnest sample (~30 nm), the strain along the out-of-plane direction is tensile, which is consistent with the strain mechanism of a hetero-epitaxial system, for which the lattice mismatch (~+13%) between the bulk VO₂ and sapphire substrate has a positive sign and should induce a tensile (positive) strain in the VO₂ thin film (Fig. 3(c)). However, for the thicker samples, a compressive strain developed; this result distinctly contradicts the strain relaxation in the conventional framework of the hetero-epitaxial system. Therefore, there must be another cause of the strain in our sputtered three thick VO₂/Al₂O₃ films. It is mentionable that the typical batch of the

samples were selected in this work, although the other batches of the samples showing the similar rules were not shown here.

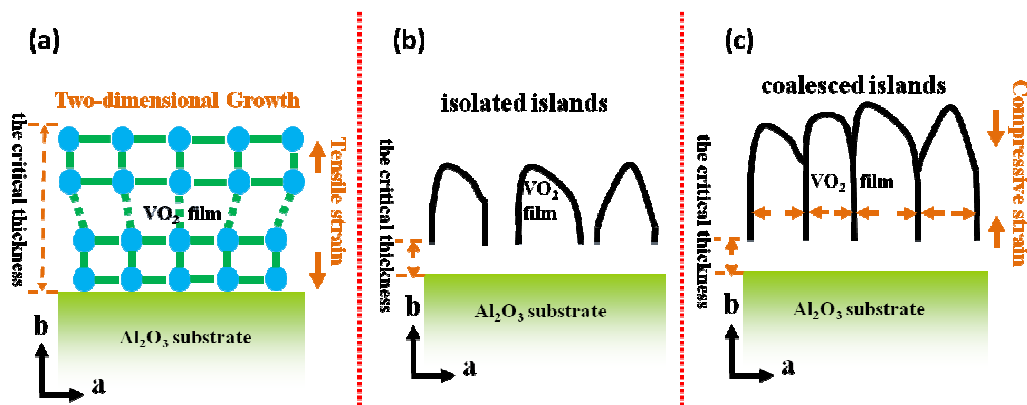


Fig. 4 (color online) Schematic diagrams of the VO_2 film surface growth modes: (a) two-dimensional growth mode, (b) and (c) island growth mode. The schematic diagrams in Fig. 4(a), (b) and (c) is not to scale.

According to previous literature³¹⁻³⁷, the anomalous strain behavior is closely related to the growth mode of the VO_2 films. At the very initial stage, under the critical thickness, the VO_2 films grow two-dimensionally on the sapphire substrate (see Fig. 4(a)). The evolution of the strain follows the mechanism of hetero-epitaxial system. Therefore, the strain state in the thinnest VO_2 films is tensile along the out-of-plane direction from the viewpoint of the lattice-mismatch-induced epitaxial strain, as illustrated in Fig. 3(c). With increasing growth time, the strain starts to relax in the thicker films, as illustrated by the dotted lines in Fig. 4(a). Simultaneously, the VO_2 nucleates discretely and forms isolated three-dimensional islands above the critical thickness (see Fig. 4(b)). At this moment, the VO_2 islands are isolated each

other and there is no strain between them. Then the islands coalesce with further increasing thickness, and for balancing the surface energy of the islands and the free energy of the grain boundaries^{33,36-38}, the lattice is extended along the in-plane direction and thus the in-plane tensile strain appears. According to the volume conservation in the solid thin films, the out-of-plane compressive strain is thus induced as shown in Fig. 4(c). This effect becomes obvious especially in the sputtering process from the metal targets at the low pressure.^{33,38} Therefore, an out-of-plane compressive strain, which balanced the in-plane tensile strain, was observed in the thicker three films and when the films become thicker, the compressive strain becomes stronger. This anomalous strain is the so-called surface-growth-mode-induced strain as reported in refs. 31 and 34.

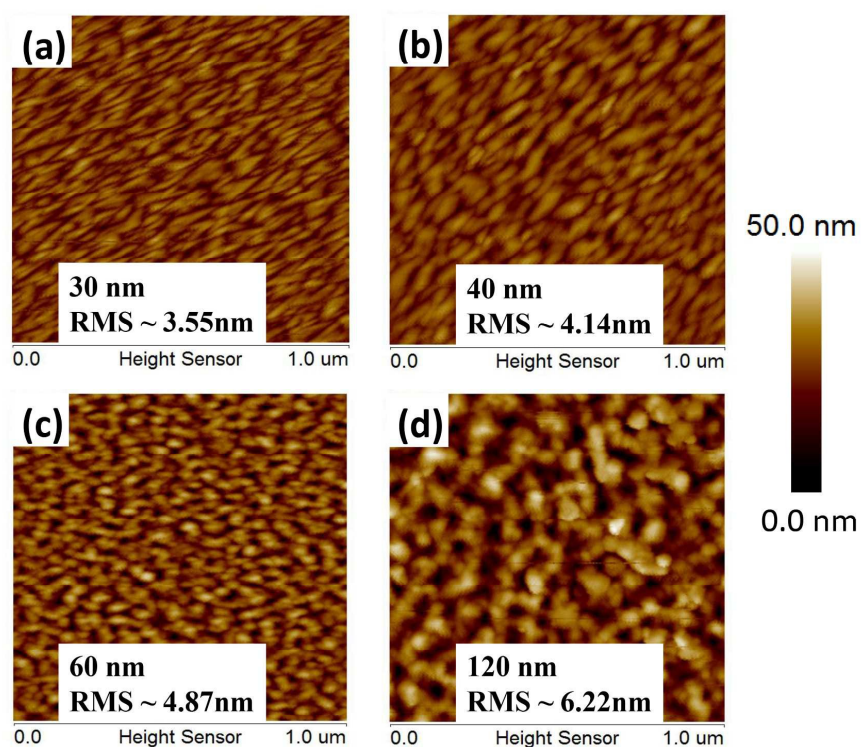


Fig. 5 (color online) Surface morphology observed using AFM and surface roughness values

(RMS: root mean square) of (a) 30-nm, (b) 40-nm, (c) 60-nm, and (d) 120-nm samples.

To verify the mechanism described above, we performed AFM studies on the VO₂ film surfaces of various thicknesses. Fig. 5 shows the surface morphologies of the four samples and clearly supports the above explanation. In Fig. 5(a) and (b), the roughness of 30-nm and 40-nm samples is less than that of 60-nm and 120-nm samples. Moreover, the islands are formed individually and appear not to overlap with each other in the thinner 30-nm and 40-nm films. The islands start to coalesce in 60-nm films, as evident from Fig. 5(c), and the three-dimensional islands become much clearer in 120-nm films, as can be observed from Fig. 5(d). This explanation has also been demonstrated experimentally in ultra-thin FeSe_{0.5}Te_{0.5}/LaAlO₃ and MgB₂/SiC epitaxial films, although an in-plane compressive strain could be expected in these films under the conventional framework of the lattice mismatch mechanism.^{33,34}

4 Conclusions

We deposited a series of VO₂ epitaxial films of different thicknesses via RF magnetron sputtering and studied their structural and electrical properties. We observed an out-of-plane tensile strain ($\sim+0.035\%$) in the thinnest VO₂ epitaxial films that was induced by an epitaxial lattice mismatch and a considerable out-of-plane compressive strain ($\sim-0.32\%$) that was induced by surface growth mode. Furthermore, the MIT temperature shifted to lower temperature with decreasing thickness, which is

attributed to modification of the orbital occupancy caused by the hetero-epitaxial strain and growth-mode-induced strains. Our results indicate that strain engineering may be served as an effective avenue for manipulating MIT behaviors of the VO₂ epitaxial films.

Acknowledgments

This work was supported by the National Basic Research Program of China (2012CB922004 and 2010CB934501), the Natural Science Foundation of China and the Anhui Province Natural Science Foundation (1508085QA06). The authors are particularly grateful to the 14B of the Shanghai Synchrotron Radiation Facility for the XRD beam time. The authors also acknowledge the partial funding from the Fundamental Research Funds for the Central Universities (WK2310000043), Scientific Research Grant of Hefei Science Center of CAS (2015SRG-HSC028) and China Postdoctoral Science Foundation (2013M540523, 2014T70597).

References

1. F. J. Morin, *Phys. Rev. Lett.*, 1959, **3**, 34.
2. T. Favaloro, J. Suh, B. Vermeersch, K. Liu, Y. Gu, L. Q. Chen, K. X. Wang and J. Wu, A. Shakouri, *Nano Lett.*, 2014, **14**, 2394.
3. G. Stefanovich, A. Pergament and D. Stefanovich, *J. Phys.: Condens. Matter*, 2000, **12**, 8837.
4. S. Lysenko, A. J. Rua, V. Vikhnin, J. Jimenez, F. Fernandez and H. Liu, *Appl. Surf. Sci.*, 2006, **252**, 5512.
5. M. Nakajima, N. Takubo, Z. Hiroi, Y. Ueda and T. Suemoto, *Appl. Phys. Lett.*, 2008, **92**, 011907.
6. B. Zhi, G. Gao, H. Xu, F. Chen, X. Tan, P. Chen, L. Wang and W. Wu, *ACS Appl. Mater. Interfaces*, 2014, **6**, 4603.
7. B. Lazarovits, K. Kim, K. Haule and G. Kotliar, *Phys. Rev. B*, 2010, **81**, 115117.
8. D. Porwal, A. C. M. Esther, I. N. Reddy, N. Sridhara, N. P. Yadav, D. Rangappa, P. Bera, C. Anandan, A. K. Sharma and A. Dey, *RSC Adv.*, 2015, **5**, 35737.
9. W. Li, S. Ji, Y. Li, A. Huang, H. Luo and P. Jin, *RSC Adv.*, 2014, **4**, 13026.
10. N. Wang, Y. Huang, S. Magdassi, D. Mandler, H. Liu and Y. Long, *RSC Adv.*, 2013, **3**, 7124.
11. L. Dai, Y. Gao, C. Cao, Z. Chen, H. Luo, M. Kanehira, J. Jin and Y. Liu, *RSC adv.*, 2012, **2**, 5265-5270.
12. X. Rui, D. Sim, C. Xu, W. Liu, H. Tan, K. Wong, H. H. Hug, T. M. Lim and Q. Yan, *RSC Adv.*, 2012, **2**, 1174-1180.

13. C. Y. Kim, S. H. Kim, S. J. Kim and K. S. An, *Appl. Surf. Sci.*, 2014, **313**, 368.
14. S. Fan, L. Fan, Q. Li, J. Liu and B. Ye, *Appl. Surf. Sci.*, 2014, **321**, 464.
15. Z. Feng, M. E. McBriarty, A. U. Mane, J. Lu, P. C. Stair, J. W. Elam and M. J. Bedzyk, *RSC Adv.*, 2014, **4**, 64608.
16. T.-H. Yang, R. Aggarwal, A. Gupta, H. Zhou, R. J. Narayan and J. Narayan, *J. Appl. Phys.*, 2010, **107**, 053514.
17. K. Martens, N. Aetukuri, J. Jeong, M. G. Samant and S. S. P. Parkin, *Appl. Phys. Lett.*, 2014, **104**, 081918.
18. K. Nagashima, T. Yanagida, H. Tanaka and T. Kawai, *Phys. Rev. B*, 2006, **74**, 172106.
19. M. M. Yang, Y. J. Yang, B. Hong, H. L. Huang, S. X. Hu, Y. Q. Dong, H. B. Wang, H. He, J. Y. Zhao, X. G. Liu, Z. L. Luo, X. G. Li, H. B. Zhang and C. Gao, *AIP Adv.*, 2015, **5**, 037114.
20. N. B. Aetukuri, A. X. Gray, M. Drouard, M. Cossale, L. Gao, A. H. Reid, R. Kukreja, H. Ohldag, C. A. Jenkins, E. Arenholz, K. P. Roche, H. A. Dürr, M. G. Samant and S. S. P. Parkin, *Nat. Phys.*, 2013, **9**, 661.
21. L. L. Fan, S. Chen, Z. L. Luo, Q. H. Liu, Y. F. Wu, L. Song, D. X. Ji, P. Wang, W. S. Chu, C. Gao, C. W. Zou and Z. Y. Wu, *Nano Lett.*, 2014, **14**, 4036.
22. Y. K. Dou, J. B. Li, M. S. Cao, D. Z. Su, F. Rehman, J. S. Zhang and H. B. Jin, *Appl. Surf. Sci.*, 2015, **345**, 232.
23. L. Liu, Y. S. Zhang and T. Y. Zhang, *J. Appl. Phys.*, 2007, **101**, 063501.
24. J. M. Booth and P. S. Casey, *Phys. Rev. Lett.*, 2009, **103**, 086402.

25. M. M. Qazilbash, M. Brehm, B. G. Chae, P. C. Ho, G. O. Andreev, B. J. Kim, S. J. Yun, A. V. Balatsky, M. B. Maple, F. Keilmann, H. T. Kim and D. N. Basov, *Science*, 2007, **318**, 1750.
26. T. Yao, X. D. Zhang, Z. H. Sun, S. J. Liu, Y. Y. Huang, Y. Xie, C. Z. Wu, X. Yuan, W. Q. Zhang, Z. Y. Wu, G. Q. Pan, F. C. Hu, L. H. Wu, Q. H. Liu and S. Q. Wei, *Phys. Rev. Lett.*, 2010, **105**, 226405.
27. S. Kittiwantanakul, S. A. Wolf and J. Lu, *Appl. Phys. Lett.*, 2014, **105**, 073112.
28. L. L. Fan, Y. F. Wu, C. Si, G. Q. Pan, C.W. Zou and Z. Y. Wu, *Appl. Phys. Lett.*, 2013, **102**, 011604.
29. L. L. Fan, S. Chen, Y. F. Wu, F. H. Chen, W. S. Chu, X. Chen, C. W. Zou and Z. Y. Wu, *Appl. Phys. Lett.*, 2013, **103**, 131914.
30. J. Cao, E. Ertekin, V. Srinivasan, W. Fan, S. Huang, H. Zheng, J. W. Yim, D. R. Khanal, D. F. Ogletree, J. C. Grossman and J. Wu, *Nat. Nanotech.*, 2009, **4**, 732.
31. H. Jalili, N. F. Heinig and K. T. Leung, *J. Chem. Phys.*, 2010, **132**, 204701.
32. A. V. Pogrebnyakov, J. M. Redwing, S. Raghavan, V. Vaithyanathan, D. G. Schlom, S. Y. Xu, Q. Li, D. A. Tenne, A. Soukiassian, X. X. Xi, M. D. Johannes, D. Kasinathan, W. E. Pickett, J. S. Wu and J. C. H. Spence, *Phys. Rev. Lett.*, 2004, **93**, 147006.
33. E. Bellingeri, I. Pallecchi, R. Buzio, A. Gerbi, D. Marre', M. R. Cimberle, M. Tropeano, M. Putti, A. Palenzona and C. Ferdeghini, *Appl. Phys. Lett.*, 2010, **96**, 102512.
34. R. Koch, D. Z. Hu and A. K. Das, *Phys. Rev. Lett.*, 2005, **94**, 146101.

35. J. Leib, R. Monig and C. V. Thompson, *Phys. Rev. Lett.*, 2009, **102**, 256101.
36. Y. J. Yang, M. M. Yang, Z. L. Luo, S. X. Hu, J. Bao, H. L. Huang, S. Zhang, J. W. Wang, P. S. Li, Y. Liu, Y. G. Zhao, X. C. Chen, G. Q. Pan, T. Jiang, Y. K. Liu, X. G. Li and C. Gao, *J. Appl. Phys.*, 2014, **115**, 173505.
37. S. C. Seel, C. V. Thompson, S. J. Hearne and J. A. Floro, *J. Appl. Phys.*, 2000, **88**, 7079.
38. C. Friesen and C. V. Thompson, *Phys. Rev. Lett.*, 2002, **89**, 126103.